



CrossMark  
click for updates

Cite this: *RSC Adv.*, 2014, 4, 40776

# Revealing the ameliorating effect of chromium oxide on a carbon nanotube catalyst in propane oxidative dehydrogenation†

Fei Ma, Shu Chen, Hang Zhou, Yanhua Li and Weimin Lu\*

Oxygenized multi-walled carbon nanotubes were modified with chromium oxide and applied in propane oxidative dehydrogenation. A propylene selectivity of 84.0% was obtained at a propane conversion of 19.8% on a Cr-1.5 wt% sample. The beneficial effect of chromium was studied by integrated techniques. X-ray photoelectron spectroscopy, and FT-IR results show that surface oxygen groups were greatly optimized as a result of chromium doping. It was also revealed that chromium improves the oxygen chemisorption properties of the catalyst, whereas the propylene desorption ability was enhanced. The superior catalytic performance was ascribed to the synergistic effect between chromium and CNTs. Moreover, as signaled from *in situ* FT-IR experiments, surface carbonyl (C=O) groups were detected to be the active sites in PODH reaction and the presence of chromium greatly facilitates C=O restoration, which as a whole determines the catalytic performance.

Received 22nd April 2014  
Accepted 26th August 2014

DOI: 10.1039/c4ra03672g

[www.rsc.org/advances](http://www.rsc.org/advances)

## 1. Instruction

Carbon nanotubes have been the focus of research on optics, electronics, magnetics and catalysis since their discovery in 1991.<sup>1–3</sup> Multi-walled carbon nanotubes possess large surface area and good thermal stability, and various functional groups could be introduced by oxidation approaches.<sup>4</sup> All these properties make them a promising candidate for the replacement of traditional catalysts. Propane oxidative dehydrogenation (PODH) represents an attractive exothermic, on-demand propylene production route.<sup>5</sup> Recently, propane activation was proved to be efficient on oxygenized CNT, and the process was coordinated by the surface carbonyl (C=O) group.<sup>6</sup> However, due to the complexity of functional groups on oxygenized CNT, lots of side products were also detected in propane oxidative dehydrogenation (PODH). In order to improve the catalytic performance, heteroatoms like P, B with lower electronegativity (series: C-2.55 > P-2.19 > B-2.04) were incorporated,<sup>7,8</sup> which modifies the surface C=O/C–O groups. The selectivity to propylene was increased, while the shortcoming of this method is that propane activation process was hindered as a result of the elimination of active C=O.<sup>9</sup> Incorporation of N atoms into the CNT framework is another approach, which could improve the propane activation due to the higher electron density, and the promoting of the dissociation of gas-phase O<sub>2</sub> to nucleophilic O<sup>2–</sup> species.<sup>10,11</sup> However, the selectivity to propylene is not satisfying until now.

Metal oxide like FeOx, VOx, TiO<sub>2</sub> have already been introduced on CNT and studied in tissue engineering,<sup>12</sup> selective oxidation<sup>13</sup> and photoconductivity<sup>14</sup> respectively. Whereas the PODH application of metal oxide doped CNT catalysts are still seldom. In this paper, CrOx was immobilized to the surface oxygen groups on CNT, and a competitive catalytic performance in PODH reaction was obtained. The relationship between oxygen transformation process on Cr–CNT catalyst and catalytic activity was also discussed for the first time.

## 2. Experimental

### 2.1 Preparation of oxidized CNT

The raw multi-walled carbon nanotubes (MWCNT) were prepared from CH<sub>4</sub> decomposition on supported Ni–MgO catalysts reported before.<sup>15</sup> The raw MWCNT were refluxed in nitric acid (8 mol L<sup>–1</sup>) at 120 °C for 12 h, and then it was cooled to r.t. and filtered with deionized water until pH = 7. The residues were dried in oven at 120 °C overnight, and the obtained black material was simplified as CNT in the text.

### 2.2 Preparation of Cr–CNT catalysts

The CNT obtained following the method above was used as the carrier. Chromium was decorated on the carrier (0.4–2.0 wt%) by wet impregnation with an aqueous solution of Cr(NO<sub>3</sub>)<sub>3</sub>·9H<sub>2</sub>O. After dispersed by ultrasound for 2 h, the obtained sample was dried in an oven at 100 °C for 4 h, and subsequently calcined at 500 °C for 4 h. The as synthesized materials were black and denoted as Cr-*x*, where *x* represents the doping weight percent.

Institute of Catalysis, Zhejiang University (Xixi Campus), Hangzhou 310028, PR China. E-mail: [luweimin@zju.edu.cn](mailto:luweimin@zju.edu.cn); Fax: +86-57188273283; Tel: +86-57188273283  
† Electronic supplementary information (ESI) available. See DOI: 10.1039/c4ra03672g

The samples were grounded and sieved to 40–60 mesh for catalytic test.

### 2.3 Catalysts characterization

Powder XRD patterns of the samples were obtained on an X-ray diffractometer (XRD, Rigaku-D/Max-B automated powder X-ray diffractometer) operating at 45 kV and 40 mA using  $\text{CuK}\alpha$  radiation ( $\lambda = 0.15418$  nm).

Transmission electron microscopic (TEM) images were obtained at 200 kV. The high-resolution TEM images were recorded on JEM-2100 instrument operated at 300 kV.

X-ray photoelectron spectroscopy (XPS) experiments were carried out on a Thermo ESCALAB 250 system with  $\text{Al K}\alpha$  radiation ( $h\nu = 1486.6$  eV).

FT-IR spectra were recorded at selected temperature on a VERTEX 70 Fourier transform instrument with a liquid-nitrogen-cooled CCD detector. During *in situ* experiment, the catalysts were pressed in self-supporting discs and pretreated in the IR cell at 250 °C for 4 h under vacuum. Gaseous propane or oxygen was controlled by mass flow meters and introduced in to the chamber at ambient temperature. Thereafter, the IR cell was heated to a selected temperature, and the IR spectra were subsequently taken.

Raman spectra of the supported chromium catalysts were obtained using a HR LabRaman 800 system equipped with a CCD detector. Each sample was pressed into a self-supporting wafer (approximately 150 mg), which was mounted on a stainless-steel adjustable holder in the center of the *in situ* cell. Propane or oxygen was controlled by mass flow meters. The spectra were recorded with a laser power of 10 mW and the 514.5 nm line of  $\text{Ar}^+$  laser.

In oxygen/propylene temperature programmed desorption experiment (TPD), all catalysts were pretreated in Ar at 250 °C for 30 min and then cooled to r.t. Oxygen/propylene was adsorbed subsequently, and with the increasing temperature from 50 to 600 °C, the desorbed molecules were analyzed by gas chromatography with a TCD detector.

The PODH reaction was carried out in a tubular fixed bed flow quartz reactor (i.d. 7.4 mm, 270 mm long) under atmosphere pressure. In a typical condition, the reaction was tested at 400 °C, GHSV = 4500  $\text{mL g}^{-1} \text{h}^{-1}$ , propane/ $\text{O}_2$  molar ratio = 2 : 1. The feedstock and reaction products were analyzed on-line by gas chromatography with two column types: Porapak QS (4.0 m  $\times$  1/8 in.) and TDX-01 (2.0 m  $\times$  1/8 in.).

## 3. Results and discussion

### 3.1 Catalytic performance

PODH reaction was examined on CNT and Cr-CNT catalysts. As shown in Fig. 1.1, propane conversion increases at higher reaction temperatures on all samples. For CNT, propane conversion was almost zero at below 350 °C, and it increases to around 5% at 400 °C. Incorporating of chromium makes the propane activation more efficient. On the catalyst of Cr-1.5, propane conversion was almost five times of that on CNT (400 °C). It needs to be mentioned that Cr-2.0 was not superior

to Cr-1.5 catalyst, indicating the excess chromium on Cr-2.0 was not active in propane reaction.

The main reaction outcomes that have been detected are propylene and COx. Propylene selectivity does not exceed 45.0% at below 400 °C on CNT (Fig. 1.2), which is similar to existed report.<sup>16</sup> Cr-CNT samples give much higher propylene selectivity than that on pure CNT, and it was still over 84.0% on Cr-1.5 at 400 °C. The generation of COx seems to be in the opposite trend to propylene (Fig. 1.3), indicating that higher temperature would make for COx. To sum up, Cr-1.5 is advantageous and gives a propylene selectivity of over 84.0% at propane conversion of 19.8%.

### 3.2 Catalysts bulk and morphology characterization

XRD patterns of different samples are shown in Fig. 2. The as obtained CNT (JCPDS: 79-1471) gives typical diffractions at  $2\theta = 26.220, 41.580, 42.581, 53.882, 78.800^\circ$ . Diffractions of  $\text{Cr}_2\text{O}_3$  (JCPDS: 82-1484,  $2\theta = 24.360, 33.400, 36.021, 50.021, 54.660, 63.301, 64.940^\circ$ ) show up in Cr-1.0, and its intensity gets stronger between Cr-1.5 and Cr-2.0. It indicates that Cr easily forms  $\text{Cr}_2\text{O}_3$  on CNT.

The morphologies of these catalysts were examined by high-resolution TEM. Fig. 3a and b show the representative image of the CNT sample. A typical herringbone-type structure with interlinked stacked space could be seen. Cr-1.5 sample (Fig. 3c) shows  $\text{Cr}_2\text{O}_3$  nanocrystals which were randomly oriented on the surface. The inset HRTEM image and FFT analysis reveals a lattice spacing of 0.362 nm, consistent with the  $d$  value of the (012) planes in  $\text{Cr}_2\text{O}_3$ .<sup>17</sup> The EDX spectrum in Fig. 3d shows the presence of Cr elements.

### 3.3 Surface oxygen groups and catalytic performance

The existent form of surface oxygen is one of the key factors that determine the catalytic reaction.<sup>18</sup> XPS experiment was implemented and the deconvoluted O1s 2p3/2 profiles are shown in Fig. 4. Binding energies of 533.42, 531.23 eV could be observed and they are accounted for C=O and C-O respectively.<sup>6,9</sup> A new peak at 529.96 eV appears on Cr-1.5, and it was associated with oxygen in  $\text{Cr}_2\text{O}_3$ .<sup>19</sup> Table 1 tells that the intensity ratio of surface  $I_{\text{C=O}}/I_{\text{C-O}}$  increases from 0.89 of CNT to 1.63 of Cr-1.5, illustrating surface oxygen groups distribution was changed after chromium was doped.

The C1s profiles of CNT could be deconvoluted into three peaks (Fig. 5): 284.7 eV (C-C), 286.6 eV (C-O) and 288.8 eV (O=C-O).<sup>20</sup> C-O and O=C-O have been proved to be anchoring sites for doping metal oxides to form C-O-M or O=C-O-M bond.<sup>14</sup> The quantitative analysis indicates that Cr-1.5 wt% doping on CNT causes O=C-O/C-O ratio increases from 0.88 to 1.65 (Table 1). This is quite consistent with the O1s analysis above.

Fig. 6 shows the IR spectra in the region of 4000–2800 and 1900–850  $\text{cm}^{-1}$  for CNT and Cr-1.5. Vibrations associated with surface C=O (1724  $\text{cm}^{-1}$ ), C=C (1580  $\text{cm}^{-1}$ ), C-O (1210  $\text{cm}^{-1}$ ) and O-H (3411  $\text{cm}^{-1}$ )<sup>21–23</sup> are observed for CNT. The comparison of the spectra of CNT and Cr-1.5 illustrates three points: (a) absorption of C=O (1724  $\text{cm}^{-1}$ ) decreases slightly, and the position shifts from 1724 to 1735  $\text{cm}^{-1}$ , suggesting that CrOx

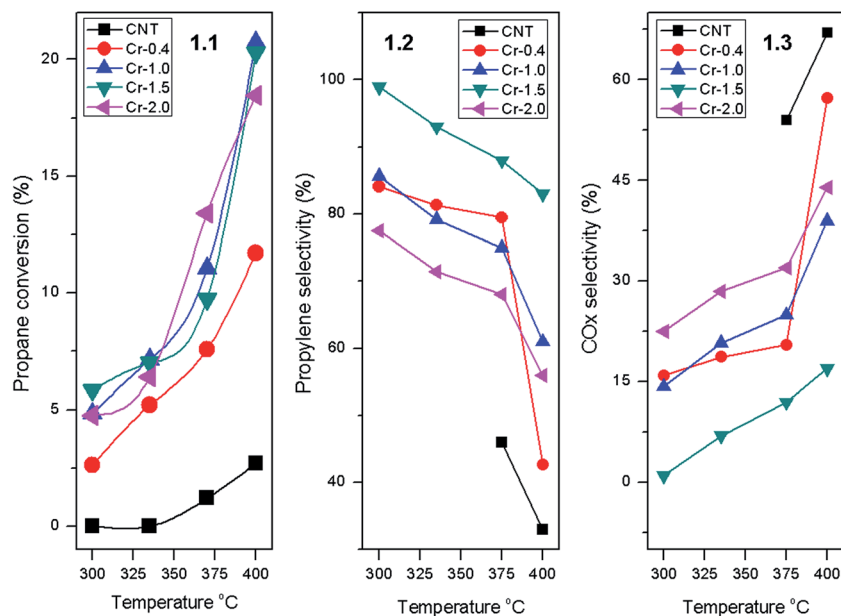


Fig. 1 PODH catalytic performance on different catalysts: (1.1) propane conversion vs. temperature, (1.2) propylene selectivity vs.  $T$ , (1.3) COx selectivity vs.  $T$ .

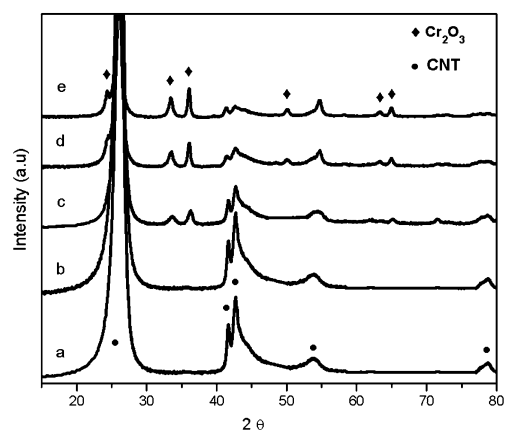


Fig. 2 XRD patterns of (a) CNT, (b) Cr-0.4, (c) Cr-1.0, (d) Cr-1.5, (e) Cr-2.0, where "●" represents CNT, "◆" represents Cr<sub>2</sub>O<sub>3</sub>.

are anchored to the CNT O–C=O groups; (b) vibrations associated with –OH (3411 cm<sup>-1</sup>) and C–O (1210 cm<sup>-1</sup>) decreased apparently, indicating that much of the surface C–O groups were decorated with CrOx; (c) C=C (1580 cm<sup>-1</sup>) stretching absorption was also weakened which might be caused by CrOx covering.

According to the XPS and FT-IR results above, it could be concluded that chromium doping decreases both C=O and C–O groups on the surface. The oxygen groups imported through HNO<sub>3</sub> oxidation on CNT are heterogeneously distributed. It seems that CrOx are more selectively attached to the C–O surface area and makes for C=O groups more predominantly.

In PODH reaction, dehydrogenation of intermediate to form propylene is widely considered as the rate determining step, and the surface that has weaker ability of propylene adsorption should avoid successive propylene reaction.<sup>24</sup> Propylene

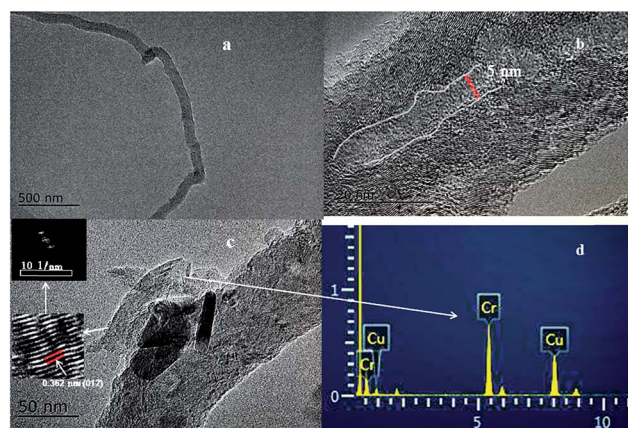


Fig. 3 TEM image and EDS analysis of CNT before and after doping: (a) CNT; (b) zoom in of (a); (c) Cr-1.5, inset is the high resolution TEM result and its FFT image; (d) EDS spectrum of selected area from image (c).

adsorption experiment was processed and shown in Fig. 7. The calculated adsorption of propylene are 20  $\mu\text{mol g}^{-1}$  for CNT and 11  $\mu\text{mol g}^{-1}$  for Cr-1.5, which confirmed the weaker ability of propylene adsorption on Cr-1.5. Combined with the catalytic performance (Fig. 1.2), propylene selectivity increases from 34.0% of CNT to around 84.0% of Cr-1.5. It might be that the modification of the surface oxygen groups greatly favors propylene desorption, and in consequence the PODH process was efficient with high selectivity.

#### 3.4 Relationship of oxygen chemisorption and dissociation with propene activation

Following the above discussion, although the quantity of surface C=O partly decreased due to chromium doping (Fig. 6),

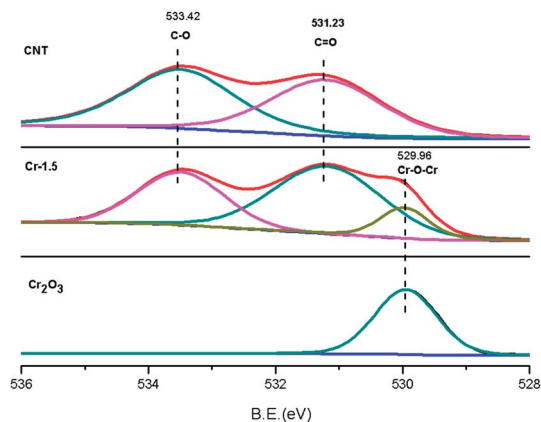


Fig. 4 O1s XPS profiles of CNT, Cr-1.5.

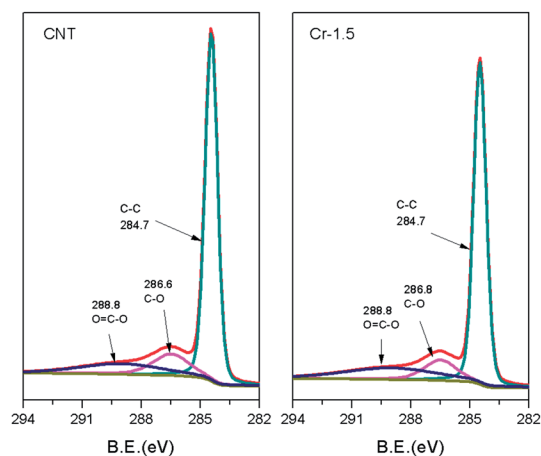


Fig. 5 C1s results of CNT, Cr-1.5.

Cr-1.5 sample exhibits propane conversion 3–5 times that of undoped CNT (Fig. 1.1). It indicates that chromium oxide must have benefited the propane activation process. The transformation of oxygen on the catalyst in PODH reaction has a significant effect on the catalytic performance.<sup>25</sup> O<sub>2</sub>-TPD was implemented to test the catalyst adsorption property of gas-phase oxygen (Fig. 7). One desorption peak centered in 90 °C superimposed with a shoulder at around 210 °C is observable on Cr-1.5, whereas there is no obvious peak on CNT in this area. It evidences that chromium doping favors the adsorption of oxygen. At temperatures over 280 °C, the peaks for the two samples are mainly associated with the decomposition of surface functional groups.<sup>16</sup> The apparent activation energy ( $E_a$ , kJ mol<sup>-1</sup>) was obtained by means of Arrhenius relationship ( $\ln r = -\frac{E_a}{RT}$ ,  $r = \text{mmol g}^{-1} \text{h}^{-1}$ ) (ref. 26) and displayed in Fig. 8. The  $E_a$  of oxygen conversion on Cr-1.5 was 111.4 kJ mol<sup>-1</sup>, which is 25.6 kJ mol<sup>-1</sup> less than that of on CNT, indicating the threshold for oxygen transformation on Cr-1.5 was lower.

The performance of propane dehydrogenation with or without oxygen on different catalysts evaluated at 10 and 400 min are listed in Table 2. When oxygen does not participate (PDH), the propane conversion was pretty low, and both CNT and Cr-1.5 materials undergo a deactivation process at around 400 min. Meanwhile the initial propylene selectivity was 87.0% on Cr-1.5, which is higher than 65.0% of CNT. The addition of oxygen in the feed stock (PODH) apparently improves the propane activation. Cr-1.5 catalyst exhibits propane conversion 4.7 times that of CNT. On the other hand, the catalytic performance, not only the conversion but also the selectivity, was

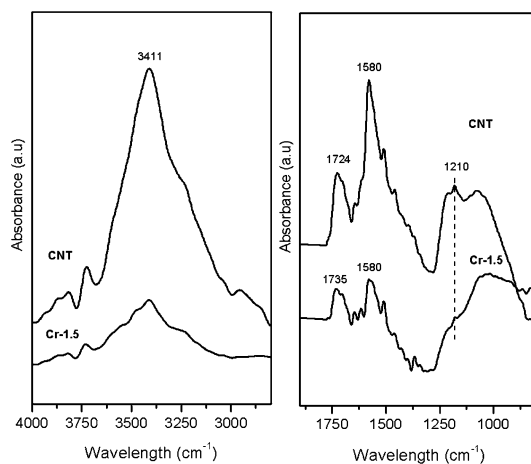


Fig. 6 FT-IR spectra of CNT and Cr-1.5.

stable and no obvious deactivation was observed on the Cr-1.5 catalyst.

To provide an intrinsic insight into the effect of chromium, we investigated the response of surface oxygen groups through *in situ* FT-IR experiment. Treatment with propane at 400 °C for 5 min, IR peaks associated with C=O (1724 cm<sup>-1</sup>), C=C (1580 cm<sup>-1</sup>) and C-O (1210 cm<sup>-1</sup>) were observed on CNT (Fig. 9a); when the processing time was extended to 400 min, C=O (1724 cm<sup>-1</sup>) absorbance fades away, and the other peaks were retained. It provides direct proof that surface C=O might be the active sites and was consumed due to the reaction with propane,

Table 1 O1s and C1s result of different samples

| Catalysts | O1s-relative atomic percentage (%) |      |      | $I_{\text{C=O}}/I_{\text{C-O}}$ from O1s | C1s-relative atomic percentage (%) |      |      | $I_{\text{C=O}}/I_{\text{C-O}}$ from C1s |
|-----------|------------------------------------|------|------|--|------------------------------------|------|------|--|
|           | Cr-O                               | C=O  | C-O  |  | C-C                                | C=O  | C-O  |  |
| CNT       | —                                  | 47.2 | 52.8 | 0.89                                     | 70.4                               | 13.9 | 15.7 | 0.88                                     |
| Cr-1.5    | 12.3                               | 54.4 | 33.3 | 1.63                                     | 67.6                               | 20.2 | 12.2 | 1.65                                     |

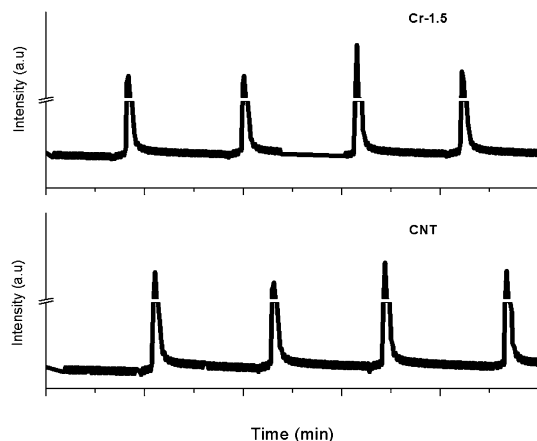


Fig. 7 Pulse adsorption of propylene on CNT and Cr-1.5 sample.

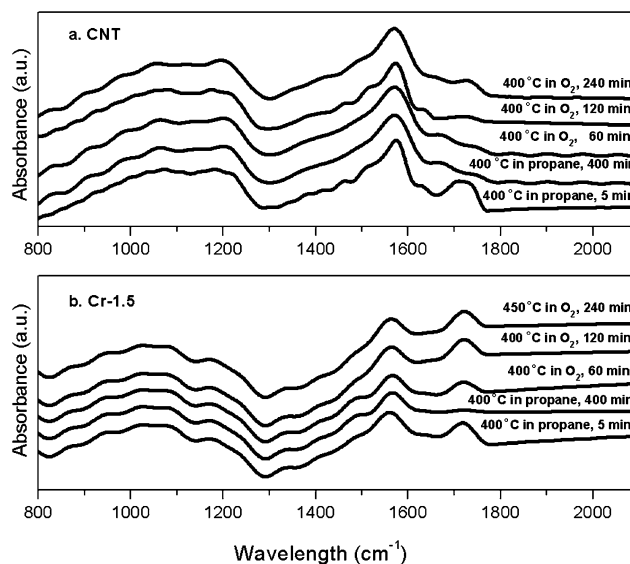


Fig. 9 FT-IR spectra of CNT and Cr-1.5 in different conditions.

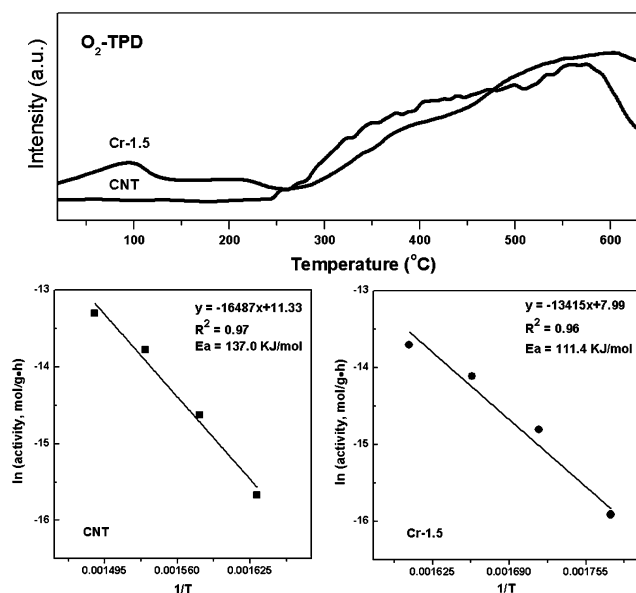


Fig. 8 O<sub>2</sub>-TPD results and the apparent activation energy ( $E_a$ ) of oxygen conversion on CNT, Cr-1.5 catalysts.

which corresponds well with the results proved by *in situ* XPS experiment.<sup>6</sup> Slight evidence of C=O peak reemerged when it was switched to O<sub>2</sub> for 120 min. The signal becomes apparent at 400 °C for 240 min, but it is still much weaker than pristine sample at 5 min. The result tells that oxygen treatment could regenerate the C=O groups consumed by propane. Incorporation of chromium greatly changes the C=O recovery situation as shown in Fig. 9b. Only in contact with oxygen for 60 min would regenerate considerable C=O peak. 120 min treatment actually gives similar intensity with pristine one. It indicates that Cr-1.5 sample exhibits much better C=O resilience property during the catalytic reaction. Combined with its catalytic performance, the effect of chromium might be reflected with the quick restoration of active sites C=O, which keeps its high conversion and selectivity. As have been discussed before, it might be that the facile oxygen chemisorption and transformation on Cr-1.5 provides good oxygen source for the regeneration of C=O. Unfortunately, the clear transformation pathway of gas-phase oxygen in our experiment remains

Table 2 Results of propane dehydrogenation and oxidative dehydrogenation on Cr-CNT catalysts at 400 °C

|                               | Propane conversion (%) |         | Propylene selectivity (%) |         | COx selectivity (%) |         |
|-------------------------------|------------------------|---------|---------------------------|---------|---------------------|---------|
|                               | 10 min                 | 400 min | 10 min                    | 400 min | 10 min              | 400 min |
| Catalysts in PDH <sup>a</sup> |                        |         |                           |         |                     |         |
| MWCNT                         | 2.0                    | 0       | 65.0                      | —       | 35.0                | —       |
| Cr-1.5                        | 1.5                    | 0.4     | 87.0                      | 36.0    | 13.0                | 64.0    |
| Catalysts in PODH             |                        |         |                           |         |                     |         |
| MWCNT                         | 4.1                    | 4.1     | 41.0                      | 40.0    | 59.0                | 60.0    |
| Cr-1.5                        | 19.4                   | 19.1    | 84.0                      | 82.0    | 16.0                | 18.0    |

<sup>a</sup> PDH means propane dehydrogenation without oxygen.

unknown. However, the process of propane dehydrogenation and the active sites restoration could be speculated: hydrogen in propane is abstracted forming a OH-group on C=O site, which is removed subsequently through dehydration; meanwhile O<sub>2</sub> might be adsorbed and dissociated on Cr<sub>2</sub>O<sub>3</sub> nanocrystals, and the as-formed oxygen species were transferred to regenerate the C=O group, which becomes a new propane adsorption site. The synergetic effect of two species has already been widely discovered in propane selective oxidation,<sup>27</sup> whereas the mechanism of the reaction in our experiment still needs exploration.

## 4. Conclusions

Through a simple impregnation process, CrOx were selectively attached to the surface of oxygenized multi-walled carbon nanotubes. The catalytic performance of CNT on PODH reaction was greatly improved by the decorating of Cr<sub>2</sub>O<sub>3</sub> nano crystals. The ameliorating effect was proved to originate mainly from two parts. Firstly, the surface oxygen groups were modified, and C=O becomes more predominant. This might explain the improved propylene selectivity, as C=O on CNT has been considered as propylene formation sites. Secondly, chromium doped sample favors propylene desorption, meanwhile oxygen chemisorption and transformation is easier. As revealed by *in situ* FT-IR experiment, C=O groups was consumed as a result of propane reaction, and chromium oxide greatly facilitates C=O regeneration. Consequently, a whole reaction picture was drawn, and synergistic effect might exist between chromium and CNT in the reaction. Despite the superior catalytic performance that we obtained, more experiments like oxygen isotropic, computational modeling would be of great help to explain the clear reaction pathway.

## Acknowledgements

The authors are grateful for the financial support of the National Natural Science Foundation of China (Grant no. 21173186).

## References

- 1 S. Iijima, *Nature*, 1991, **354**, 56–58.
- 2 H. Dai, J. H. Hafner, A. G. Rinzler, D. T. Colbert and R. E. Smalley, *Nature*, 1996, **384**, 147–150.
- 3 T. Ebbesen, H. Lezec, H. Hiura, J. Bennett, H. Ghaemi and T. Thio, *Nature*, 1996, **382**, 54–56.
- 4 V. Datsyuk, M. Kalyva, K. Papagelis, J. Parthenios, D. Tasis, A. Siokou, I. Kallitsis and C. Galiotis, *Carbon*, 2008, **46**, 833–840.
- 5 F. Cavani, N. Ballarini and A. Cericola, *Catal. Today*, 2007, **127**, 113–131.
- 6 J. Zhang, X. Liu, R. Blume, A. Zhang, R. Schlögl and D. S. Su, *Science*, 2008, **322**, 73–77.
- 7 L. Yang, S. Jiang, Y. Zhao, L. Zhu, S. Chen, X. Wang, Q. Wu, J. Ma, Y. Ma and Z. Hu, *Angew. Chem., Int. Ed.*, 2011, **123**, 7270–7273.
- 8 E. Cruz-Silva, D. A. Cullen, L. Gu, J. M. Romo-Herrera, E. Muñoz-Sandoval, F. López-Urías, B. G. Sumpter, V. Meunier, J.-C. Charlier, D. J. Smith, H. Terrones and M. Terrones, *ACS Nano*, 2008, **2**, 441–448.
- 9 B. Frank, J. Zhang, R. Blume, R. Schlögl and D. S. Su, *Angew. Chem., Int. Ed.*, 2009, **48**, 6913–6917.
- 10 C. Gao, Y. Z. Jin, H. Kong, R. L. Whitby, S. F. Acquah, G. Chen, H. Qian, A. Hartschuh, S. Silva and S. Henley, *J. Phys. Chem. B*, 2005, **109**, 11925–11932.
- 11 J. Liu, H. Liu, Y. Zhang, R. Li, G. Liang, M. Gauthier and X. Sun, *Carbon*, 2011, **49**, 5014–5021.
- 12 C. Cunha, S. Panseri, D. Iannazzo, A. Piperno, A. Pistone, M. Fazio, A. Russo, M. Marcacci and S. Galvagno, *Nanotechnology*, 2012, **23**, 465102.
- 13 B. Frank, M. Morassutto, R. Schomäcker, R. Schlögl and D. S. Su, *ChemCatChem*, 2010, **2**, 644–648.
- 14 J. Yu, T. Ma and S. Liu, *Phys. Chem. Chem. Phys.*, 2011, **13**, 3491–3501.
- 15 P. Chen, H.-B. Zhang, G.-D. Lin, Q. Hong and K. Tsai, *Carbon*, 1997, **35**, 1495–1501.
- 16 C. Chen, J. Zhang, B. Zhang, C. Yu, F. Peng and D. Su, *Chem. Commun.*, 2013, **49**, 8151–8153.
- 17 K. Jiao, B. Zhang, B. Yue, Y. Ren, S. Liu, S. Yan, C. Dickinson, W. Zhou and H. He, *Chem. Commun.*, 2005, 5618–5620.
- 18 G. I. Panov, A. K. Uriarte, M. A. Rodkin and V. I. Sobolev, *Catal. Today*, 1998, **41**, 365–385.
- 19 M. Witthaut, R. Cremer, K. Reichert and D. Neuschütz, *Microchim. Acta*, 2000, **133**, 191–196.
- 20 R. Nie, J. Wang, L. Wang, Y. Qin, P. Chen and Z. Hou, *Carbon*, 2012, **50**, 586–596.
- 21 W. Qi, W. Liu, B. Zhang, X. Gu, X. Guo and D. Su, *Angew. Chem., Int. Ed.*, 2013, **52**, 14224–14228.
- 22 B. Huang, R. Huang, D. Jin and D. Ye, *Catal. Today*, 2007, **126**, 279–283.
- 23 L. Cao, H. Chen, M. Wang, J. Sun, X. Zhang and F. Kong, *J. Phys. Chem. B*, 2002, **106**, 8971–8975.
- 24 C. Coperet, *Chem. Rev.*, 2009, **110**, 656–680.
- 25 G. I. Panov, K. A. Dubkov and E. V. Starokon, *Catal. Today*, 2006, **117**, 148–155.
- 26 K. Miura, *Energy Fuels*, 1995, **9**, 302–307.
- 27 U. S. Ozkan and R. B. Watson, *Catal. Today*, 2005, **100**, 101–114.